



This is a repository copy of *Improved power computation method for droop-controlled single-phase VSIs in standalone microgrid considering non-linear loads*.

White Rose Research Online URL for this paper:

<https://eprints.whiterose.ac.uk/207552/>

Version: Published Version

Article:

Kherbachi, A. orcid.org/0000-0002-6166-7744, Chouder, A., Bendib, A. et al. (1 more author) (2023) Improved power computation method for droop-controlled single-phase VSIs in standalone microgrid considering non-linear loads. *IET Generation, Transmission and Distribution*, 17 (7). pp. 1442-1460. ISSN 1751-8687

<https://doi.org/10.1049/gtd2.12749>

Reuse

This article is distributed under the terms of the Creative Commons Attribution-NonCommercial-NoDerivs (CC BY-NC-ND) licence. This licence only allows you to download this work and share it with others as long as you credit the authors, but you can't change the article in any way or use it commercially. More information and the full terms of the licence here: <https://creativecommons.org/licenses/>

Takedown

If you consider content in White Rose Research Online to be in breach of UK law, please notify us by emailing eprints@whiterose.ac.uk including the URL of the record and the reason for the withdrawal request.



eprints@whiterose.ac.uk
<https://eprints.whiterose.ac.uk/>

ORIGINAL RESEARCH

Improved power computation method for droop-controlled single-phase VSIs in standalone microgrid considering non-linear loads

 Abdelhamid Kherbachi¹  | Aissa Chouder² | Ahmed Bendib³ | Hafiz Ahmed⁴ 
¹Centre de Développement des Energies Renouvelables, Bouzaréah, Algiers, Algeria

²Electrical Engineering Laboratory (LGE), University Mohamed Boudiaf of Msila BP166, Msila, Algeria

³SET Laboratory, Electronics Department, Blida University, Msila, Algeria

⁴Nuclear Futures Institute, Bangor University, Bangor, UK
Correspondence
 Hafiz Ahmed, Nuclear Futures Institute, School of Computer Science and Electronic Engineering, Dean Street, Bangor LL57 1UT, UK.
Email: hafiz.h.ahmed@icee.org
Funding information

Welsh European Funding Office (WEFO)

Abstract

Computation of active and reactive powers is a crucial step in droop-controlled single-phase voltage source inverters (VSIs) in standalone microgrid since the performance and stability of the power-sharing strategy are strongly influenced by its speed and accuracy, especially in the case of non-linear loads. Here, an improved performance of power-sharing among single-phase droop-controlled VSIs in an islanded microgrid, considering DC component and nonlinear loads is presented. To achieve this goal, an enhanced power-sharing control scheme including a Multiple Enhanced Second-Order Generalized Integrator Frequency-Locked Loop (MESOGI-FLL) for power calculation is proposed. As a result, the proposed power computation technique provides high rejection capability of DC component and current harmonics, hence, perfect estimation of the fundamental component of the inverter output current and its 90° phase-shifted component. This strategy makes the power calculation method-based control scheme immune to disturbance effects of the DC component and the high current harmonics. Detailed analysis, mathematical modelling of MESOGI, as well as a comparison with recent methods, are also provided. Simulation and experimental tests were carried out and the obtained results have shown the effectiveness and robustness of the proposed power-sharing controller even under nonlinear load operating conditions.

1 | INTRODUCTION

Primary control as a local controller of a microgrid (MG) is the first control level that should be addressed in order to guarantee load sharing between parallelized VSIs during the autonomous operating mode [1, 2]. At this control stage, the droop control strategy is the most adopted control approach due to its advantages in terms of ease of implementation and the required references are calculated locally [3–5]. Based on such a control strategy, the frequency and amplitude references of the inverter output voltage are immediately obtained by using the measured real and reactive powers [6, 7]. This immediate effect makes the computation of average real and reactive powers a crucial step since the stability and performance of the droop control are strongly influenced by its speed and accuracy, especially in the case of nonlinear loads [8]. In fact, under such

conditions, the traditional methods that generally introduce a low-pass filter (LPF) to mitigate undesirable distortions, cannot guarantee fast and accurate power calculation. In addition, the DC component is another issue that has a critical influence on the power calculation performances and might worsen system stability. Therefore, the design of a power computation scheme with improved performance should be addressed by considering the aforementioned issues.

Traditional calculation methods for single-phase droop-controlled systems compute the instantaneous active and reactive powers by the multiplications of the inverter measured output current with the inverter output voltage, and with its 90° phase-shifted component generated by a quarter-cycle delay unit [6, 9–12]. In such a computation approach, a mandatory LPF is needed in order to eliminate the double frequency component, resulting from the product of the output voltage with

This is an open access article under the terms of the [Creative Commons Attribution-NonCommercial-NoDerivs](https://creativecommons.org/licenses/by-nc-nd/4.0/) License, which permits use and distribution in any medium, provided the original work is properly cited, the use is non-commercial and no modifications or adaptations are made.

© 2023 The Authors. *IET Generation, Transmission & Distribution* published by John Wiley & Sons Ltd on behalf of The Institution of Engineering and Technology.

the components of the output current and thus obtaining the average active and reactive powers [9]. In other methods, additional quarter-cycle delay units have been introduced to handle the double-frequency components cancellation [13, 14]. Instead of using delay units and avoiding their inherent performance degradation problems [8], advanced power calculation methods have been proposed [15–22]. Among these methods, intended for three and single-phase systems are those based on the SOGI technique. These methods use SOGI as an estimator of voltage and current components as well as the double frequency components estimation/rejection. In [15] and [16], the SOGI is introduced to extract the direct and quadrature components of both output voltage and current. Then, these components are employed to calculate the average powers in the $\alpha\beta$ -frame [17]. The method presented in [18], calculates the instantaneous powers similar to the conventional method, but it introduces two SOGI blocks to extract the oscillating components where their frequency is double of the fundamental frequency and subtract them from the instantaneous powers. The authors in [19] have proposed an enhanced power calculation method, which uses SOGI to estimate the $\alpha\beta$ -components of the inverter output voltage and current. The direct product of the voltage components with the current components is performed, and average active and reactive powers are obtained through second-order LPFs. These power calculation methods based on SOGI can be easily implemented without delay as well as they have the advantages of fast transient response and accepted rejection capability of load distortions. Nevertheless, LPF is still necessary for such methods for proper harmonics rejection under highly distorted voltage and current. However, the LPF limits the transient response speed of the power calculation and may degrade the power-sharing stability. In order to avoid using LPF, solutions based on discrete Fourier transform (DFT), least mean squares (LMS), and moving-average approaches have been proposed to achieve average active and reactive powers [20–22]. The main drawback of these methods is that they need more computation time to perform P/Q calculations. In addition, a particular drawback of the DFT-based method is that it introduces a significant time delay in the system process. Furthermore, the LMS based-method has a poor dynamic response regarding the overshoot term.

In general, all the methods mentioned above have not properly taken into consideration the case of nonlinear load conditions and undesirable output voltage and current inherent disturbances. Therefore, power calculation with good performance and desired speed cannot be guaranteed. In addition, the DC component, which may be caused by MG faults, conversion process, measurement devices, and imperfect PWM patterns, is one of the major issues that may affect the performance of these methods and consequently worsen the stability of the parallelized system.

For these reasons, recent approaches have been proposed in the literature to overcome these issues and ensure fast and accurate calculation of average powers while considering nonlinear loads. These methods are designed by introducing an advanced SOGI-based scheme suitable for DC offset and nonlinear load harmonic rejection capability. For instance, a power

calculation method based on the double SOGI (DSOGI) strategy is presented in [23]. This method is similar to the one presented in [15], but it introduces the DSOGI to provide a perfectly filtered direct fundamental component of the output current by ensuring the high rejection of the DC component and high current harmonics. This component is multiplied by the voltage fundamental component extracted using standard SOGI, and the average powers are obtained after removing the double-frequency component. Roughly speaking, in the case of the presence of the DC component in the inverter voltage, the performance of this method might be questionable due to the sensibility of the SOGI to such a disturbance [24]. In [25], the average powers are achieved through SOGI that acts as an LPF, where its inputs are the real and reactive power obtained by multiplying the fundamental $\alpha\beta$ current components provided by another SOGI that acts as a band-pass filter (BPF), with the $\alpha\beta$ voltage components. Although this method, which has been applied to a three-phase system, has provided fast power calculation, the presence of the DC component in the inverter voltage may lead to inaccurate power calculation with undesirable oscillations. In [26], an ESOGI-FLL-based power calculation method in $\alpha\beta$ -frame is proposed, in which the ESOGI is applied for the estimation of both voltage and current $\alpha\beta$ components. Although this method has addressed the DC component effect cancelation, proper harmonics rejection in the case of nonlinear load cannot be guaranteed. In [27], an approach for power calculation is proposed by using the n-SOGI strategy, which is applied to extract the orthogonal fundamental components of both inverter output voltage and current. These components are used to calculate the voltage amplitude and phase, then, the active and reactive power can be obtained by exploiting sine and cosine functions. Despite this method have presented a performance enhancement of the power calculation under DC component and nonlinear load conditions, it needs more computational time due to the use of the trigonometric functions, therefore, a control with high computation burden is expected.

Here, we propose a substantial improvement of the power-sharing performance among single-phase droop-controlled VSIs in an islanded microgrid considering DC offset and non-linear load disturbances. To achieve this objective, the following contributions are made. First, an improved power calculation method based on Multiple Enhanced SOGI-FLL (MESOGI-FLL) is developed. The proposed MESOGI-FLL strategy provides high rejection capability of DC offset component and current harmonics. As a result, an accurate estimation of the fundamental direct component of the inverter output current and its 90° phase-shifted component, which are mandatory for power calculation, is guaranteed. Second, the details of mathematical model derivation of the MESOGI are presented in order to evaluate the expected performances. Third, a simulation study evaluating the performance of the proposed power calculation method in comparison to the recent methods is carried out. Fourth, simulation and experimental tests are performed and the obtained results show the effectiveness and robustness of the proposed power-sharing controller even under nonlinear load operating conditions.

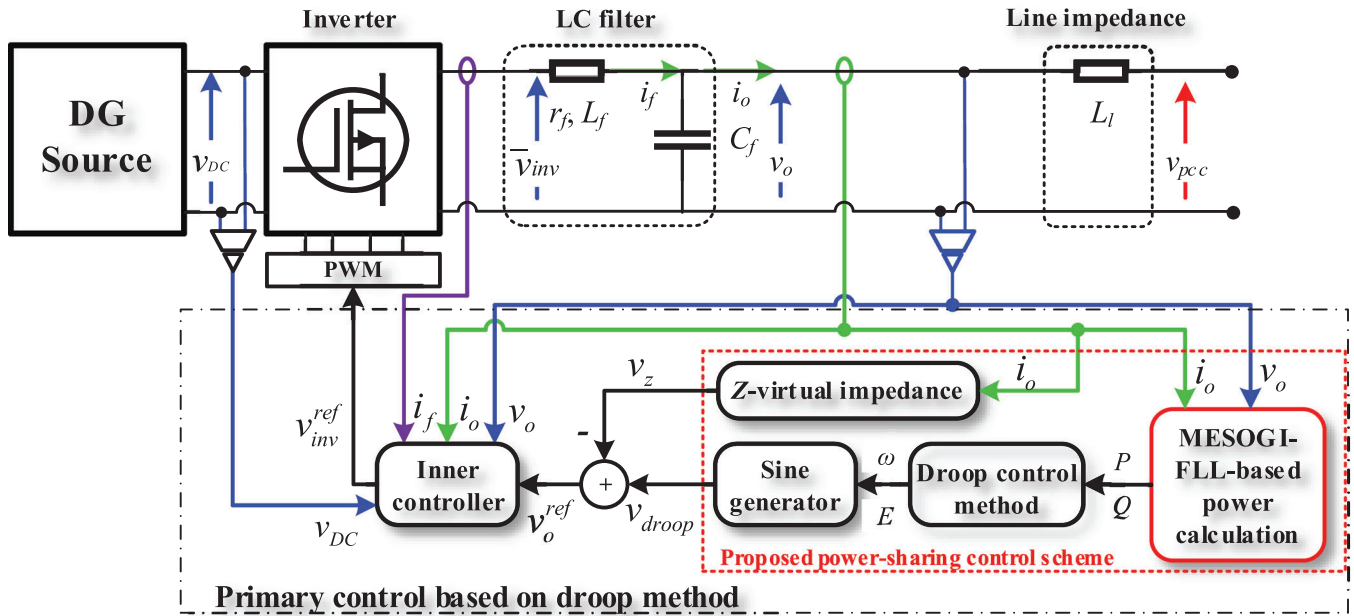


FIGURE 1 The proposed power-sharing approach-based primary control for a single-phase inverter

The rest of this paper is structured as follows. Section 2 gives the general architecture of the studied system and the corresponding control modules. Section 3 details the mathematical derivations and the transfer functions of the proposed power calculation method. Simulation results considering linear and non-linear loads are highlighted in Section 4. The experimental setup validating the proposed power calculation method is presented in Section 5. Finally, in Section 6 some conclusions are derived.

2 | DROOP-OPERATED SINGLE-PHASE VSIS

Figure 1 shows a schematic diagram of the proposed power-sharing approach-based primary control scheme for a single-phase VSI in islanded MG. The adopted control strategy is the droop method where the authors propose a new enhanced power calculation algorithm based on MESOGI-FLL in order to provide accurate average P/Q powers. The calculated powers are fed to the droop controller to generate the frequency and amplitude references. These generated references are processed by a sinusoidal signal generator to produce the fundamental component reference of the inverter output voltage. Moreover, MESOGI-FLL is used to extract the in-phase component, the orthogonal component and its harmonics components for computing the virtual impedance voltage, to be subtracted from the fundamental output voltage reference given by the droop control module. The new delivered voltage reference is manipulated by a multi-loop inner controller and a PWM to control the inverter switches.

In this control scheme, the droop control is responsible for controlling the real and reactive power-sharing among the parallelized VSIs by using the frequency and amplitude droop characteristics defined as follows:

$$\begin{cases} \omega = \omega_n - mP \\ E = E_n - nQ \end{cases} \quad (1)$$

where ω , E , ω_n , and E_n are the frequency and amplitude references and their nominal values, and n and m are the droop gains.

The sine generator provides the output voltage reference, v_{droop} , given by the following equation:

$$v_{droop}(t) = E \times \sin(\omega \times t) \quad (2)$$

The virtual impedance control loop, which is implemented based on the MESOGI-FLL, is introduced to improve the power-sharing accuracy. So, the output of the virtual impedance control loop can be obtained as follows:

$$v_z = r_v i_o - L_v \omega (i_{\beta-1} + 3i_{\beta-3} + 5i_{\beta-5} + 7i_{\beta-7}) \quad (3)$$

where r_v and L_v are the virtual resistor and inductor, i_o is the actual input current, and $i_{\beta-1}$, $i_{\beta-3}$, $i_{\beta-5}$, and $i_{\beta-7}$ are the current quadrature fundamental, 3rd, 5th, and 7th components.

Accordingly, the new output voltage reference can be derived as:

$$v_o^{ref} = v_{droop} - v_z \quad (4)$$

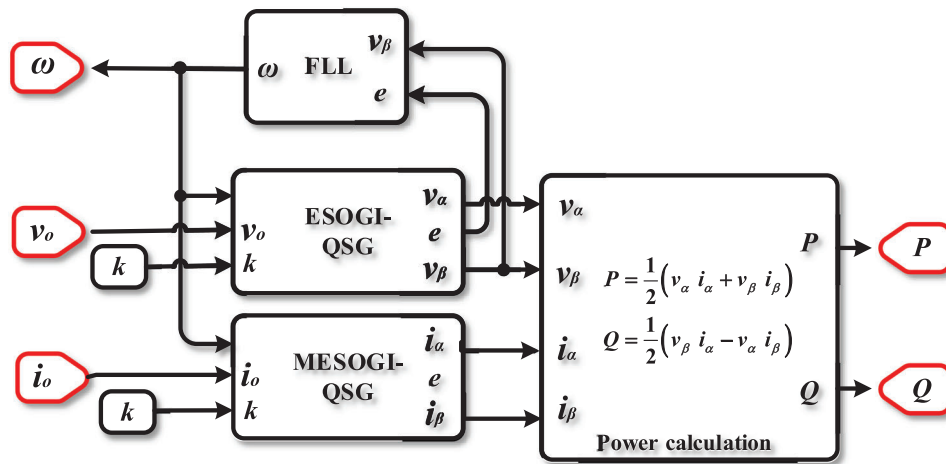


FIGURE 2 Schematic diagram of the proposed power calculation method based on MESOGI-FLL

The inner controller is in charge of regulating the output voltage of the inverter to its generated voltage reference given by (4). This control stage consists of an inner current control loop and an outer voltage control loop. For more details about this control stage refer to [28].

3 | PROPOSED POWER CALCULATION METHOD

This section deals with the design, modelling, and analysis of a proposed power calculation method based on the MESOGI-FLL scheme intended for single-phase droop-operated VSIs. Figure 2 shows the structure of the proposed power calculation module, which consists of; (i) a MESOGI-QSG module; that constitutes multiple ESOGI-QSG connected in parallel; intended to accurately extract the direct and the quadrature fundamental components of the inverter output current; (ii) an ESOGI-QSG module suitable for DC offset rejection and responsible for estimating the fundamental components of the inverter voltage; (iii) an FLL unit to adapt the centre frequency of both MESOGI and ESOGI to frequency changes. The estimated fundamental components of the inverter voltage and current are exploited to calculate the average active and reactive powers in the $\alpha\beta$ -frame. In particular, MESOGI can provide a fast estimation of the current components with high DC component and harmonic rejection capabilities under nonlinear load conditions. The same capabilities can be provided by ESOGI regarding voltage components estimation. Hence, the proposed calculation algorithm can ensure fast and accurate average active and reactive powers calculation, with good transient performance even in the case of highly distorted current. In addition, as the MESOGI-FLL does not process any trigonometric functions, it can be easily implemented with a reduced computation time.

In the next section, a detailed description of the proposed MESOGI-QSG will be given. The modelling procedure

for obtaining the dynamic model of the MESOGI regarding i_{α} , i_{β} , and i_{DC} estimation, will also be provided. We note that i_{α} , i_{β} , and i_{DC} are the direct, orthogonal, and DC components respectively of the inverter output current.

3.1 | Multiple-ESOGI modelling and analysis

3.1.1 | Structure of the MESOGI

Figure 3a shows the adopted MESOGI-QSG structure to estimate precisely the current components under worst-case distorted conditions (DC component and nonlinear load). This proposed structure includes n ESOGI-QSG, as shown in Figure 3a, connected in parallel. The first involved ESOGI-QSG is constructed by adding a rejection/estimation unit (LPF) to the standard SOGI-QSG as shown in Figure 3b. While the rest of ESOGI (eSOGI) units introduce the DC component, estimated by the first one, as an input to be subtracted from the orthogonal component. The ESOGI (or eSOGI) units provide total rejection of the DC component as well as its effect on the output components [20]. Each eSOGI adaptive filter, in the proposed structure, is tuned to a particular frequency, multiple of the fundamental frequency, by multiplying the fundamental frequency, estimated by the FLL, by a coefficient that determines the order of the assigned harmonic. Furthermore, the gain “ k ” of each eSOGI is divided by the order of such a coefficient in order to maintain the same settling time of the transient response of all the eSOGI-QSG (see Appendix A). The input current for each ESOGI (eSOGI) unit is calculated by subtracting all the rest of the in-phase output components of the other units from the actual input current. In this regard, the input current of each eSOGI is cleaned up, after a transient process, from the harmonic components estimated by the rest of the blocks, which will reject the harmonic distortions at its output.

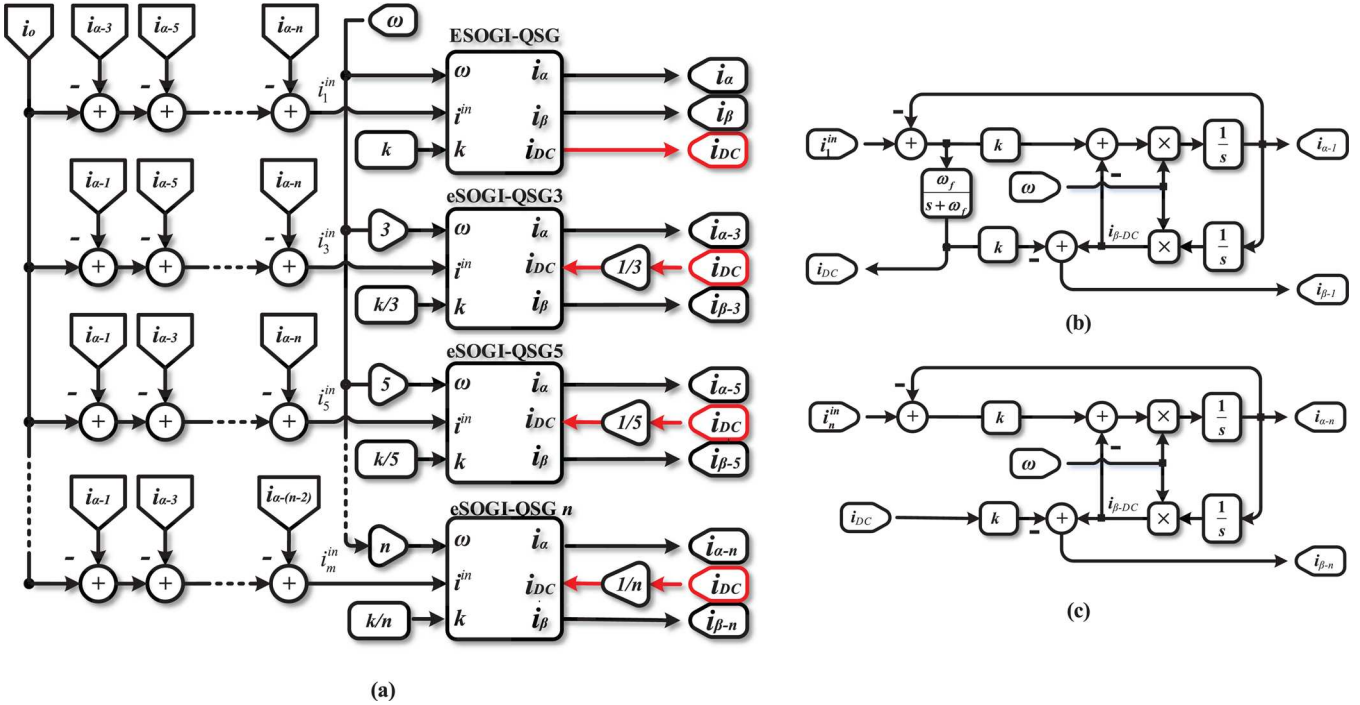


FIGURE 3 Structure of (a) the MESOGI-QSG method, (b) the ESOGI-QSG method, and (c) the eSOGI-QSG method

3.1.2 | MESOGI Modelling

According to the structure given in Figure 3b, the mathematical expressions relating the output current components ($i_{\alpha-n}$, $i_{\beta-n}$, and i_{DC}) of each eSOGI unit to its input, i_n^{in} , can be given as follows:

$$\begin{cases} i_{\alpha-n} = G_{\alpha-n} i_n^{in} \\ i_{\beta-n} = G_{\beta-n} i_n^{in} - (k/n) i_{DC} \\ i_{DC} = G_{DC} (i_1^{in} - i_{\alpha-1}) \end{cases} \quad (5)$$

being n the harmonic's order, i_1^{in} and $i_{\alpha-1}$ the fundamental component of the input current and the in-phase current, and $G_{\alpha-n}$, $G_{\beta-n}$, and G_{DC} are the transfer functions of the ESOGI defined as follows:

$$\begin{cases} G_{\alpha-n} = \frac{i_{\alpha-n}}{i_n^{in}} = \frac{k\omega s}{s^2 + k\omega s + n^2\omega^2} \\ G_{\beta-n} = \frac{i_{\beta-n-DC}}{i_n^{in}} = \frac{k n \omega^2}{s^2 + k\omega s + n^2\omega^2} \\ G_{DC} = \frac{i_{DC}}{i_1^{in} - i_{\alpha-1}} = \frac{\omega_f}{s + \omega_f} \end{cases} \quad (6)$$

where s denotes the Laplace operator, ω is the centre frequency generated by the FLL block, and ω_f is the cutoff frequency of the LPF.

In addition, from Figure 3a, the relation between the input current i_n^{in} of each ESOGI unit and the actual input current i_o

can be derived as follows:

$$i_j^{in} = i_o - \sum_{\substack{p=0 \\ i=2p+1 \\ i \neq j}}^n i_{\alpha-i} \quad (7)$$

Equation (7) can be written in matrix form as follows:

$$\begin{bmatrix} i_1 \\ i_3 \\ i_5 \\ \vdots \\ i_n \end{bmatrix}^{in} = - \begin{bmatrix} 0 & 1 & 1 & \cdots & 1 \\ 1 & 0 & 1 & \cdots & 1 \\ 1 & 1 & 0 & \cdots & 1 \\ \vdots & \vdots & 1 & \ddots & \vdots \\ 1 & 1 & 1 & \cdots & 0 \end{bmatrix} \begin{bmatrix} i_{\alpha-1} \\ i_{\alpha-3} \\ i_{\alpha-5} \\ \vdots \\ i_{\alpha-n} \end{bmatrix} + \begin{bmatrix} 1 \\ 1 \\ 1 \\ \vdots \\ 1 \end{bmatrix} i_o \quad (8)$$

Based on (5), the transfer functions of the output components of the eSOGI adaptive filters can be represented in matrix form as follows:

- a. For the output components $i_{\alpha-n}$, which is in-phase with the input signal i_n^{in} of each eSOGI block:

$$\begin{bmatrix} i_{\alpha-1} \\ i_{\alpha-3} \\ i_{\alpha-5} \\ \vdots \\ i_{\alpha-n} \end{bmatrix} = \begin{bmatrix} G_{\alpha-1} & 0 & 0 & \cdots & 0 \\ 0 & G_{\alpha-3} & 0 & \cdots & 0 \\ 0 & 0 & G_{\alpha-5} & \cdots & 0 \\ \vdots & \vdots & \vdots & \ddots & \vdots \\ 0 & 0 & 0 & \cdots & G_{\alpha-n} \end{bmatrix} \begin{bmatrix} i_1 \\ i_3 \\ i_5 \\ \vdots \\ i_n \end{bmatrix}^{in} \quad (9)$$

b. For the output components $i_{\beta-n}$, which is in-quadrature phase with the input signal i_n^{in} of each eSOGI block:

$$\begin{bmatrix} i_{\beta-1} \\ i_{\beta-3} \\ i_{\beta-5} \\ \vdots \\ i_{\beta-n} \end{bmatrix} = \begin{bmatrix} G_{\beta-1} & 0 & 0 & \cdots & 0 \\ 0 & G_{\beta-3} & 0 & \cdots & 0 \\ 0 & 0 & G_{\beta-5} & \cdots & 0 \\ \vdots & \vdots & \vdots & \ddots & \vdots \\ 0 & 0 & 0 & \cdots & G_{\beta-n} \end{bmatrix} \begin{bmatrix} i_1^{in} \\ i_3 \\ i_5 \\ \vdots \\ i_n \end{bmatrix} - \begin{bmatrix} k \\ k/3 \\ k/5 \\ \vdots \\ k/n \end{bmatrix} i_{DC} \tag{10}$$

c. For the output components i_{DC} , which is the DC component related to the input signal i_n^{in} and the direct output components $i_{\alpha-n}$ of each eSOGI block:

$$i_{DC} = G_{DC} [1 \quad 0 \quad 0 \quad \cdots \quad 0] \begin{bmatrix} i_1^{in} \\ i_3 \\ i_5 \\ \vdots \\ i_n \end{bmatrix} - \begin{bmatrix} i_{\alpha-1} \\ i_{\alpha-3} \\ i_{\alpha-5} \\ \vdots \\ i_{\alpha-n} \end{bmatrix} \tag{11}$$

By substituting (8) into (9)–(11), the closed-loop transfer functions of the output components of the proposed structure can be expressed as follows:

a. For the output components $i_{\alpha-n}$

$$\begin{bmatrix} i_{\alpha-1} \\ i_{\alpha-3} \\ i_{\alpha-5} \\ \vdots \\ i_{\alpha-n} \end{bmatrix} = \begin{bmatrix} 1 & G_{\alpha-1} & G_{\alpha-1} & \cdots & G_{\alpha-1} \\ G_{\alpha-3} & 1 & G_{\alpha-3} & \cdots & G_{\alpha-3} \\ G_{\alpha-5} & G_{\alpha-5} & 1 & \cdots & G_{\alpha-5} \\ \vdots & \vdots & \vdots & \ddots & \vdots \\ G_{\alpha-n} & G_{\alpha-n} & G_{\alpha-n} & \cdots & 1 \end{bmatrix}^{-1} \begin{bmatrix} G_{\alpha-1} \\ G_{\alpha-3} \\ G_{\alpha-5} \\ \vdots \\ G_{\alpha-n} \end{bmatrix} i_o \tag{12}$$

b. For the output components $i_{\beta-n}$

$$\begin{bmatrix} i_{\beta-1} \\ i_{\beta-3} \\ i_{\beta-5} \\ \vdots \\ i_{\beta-n} \end{bmatrix} = - \begin{bmatrix} 0 & G_{\beta-1} & G_{\beta-1} & \cdots & G_{\beta-1} \\ G_{\beta-3} & 0 & G_{\beta-3} & \cdots & G_{\beta-3} \\ G_{\beta-5} & G_{\beta-5} & 0 & \cdots & G_{\beta-5} \\ \vdots & \vdots & \vdots & \ddots & \vdots \\ G_{\beta-n} & G_{\beta-n} & G_{\beta-n} & \cdots & 0 \end{bmatrix} \begin{bmatrix} i_1^{in} \\ i_3 \\ i_5 \\ \vdots \\ i_n \end{bmatrix}$$

$$\begin{aligned} & \times \begin{bmatrix} 1 & G_{\alpha-1} & G_{\alpha-1} & \cdots & G_{\alpha-1} \\ G_{\alpha-3} & 1 & G_{\alpha-3} & \cdots & G_{\alpha-3} \\ G_{\alpha-5} & G_{\alpha-5} & 1 & \cdots & G_{\alpha-5} \\ \vdots & \vdots & \vdots & \ddots & \vdots \\ G_{\alpha-n} & G_{\alpha-n} & G_{\alpha-n} & \cdots & 1 \end{bmatrix}^{-1} \\ & \times \begin{bmatrix} G_{\alpha-1} \\ G_{\alpha-3} \\ G_{\alpha-5} \\ \vdots \\ G_{\alpha-n} \end{bmatrix} + \begin{bmatrix} G_{\beta-1} \\ G_{\beta-3} \\ G_{\beta-5} \\ \vdots \\ G_{\beta-n} \end{bmatrix} i_o - \begin{bmatrix} k \\ k/3 \\ k/5 \\ \vdots \\ k/n \end{bmatrix} i_{DC} \end{aligned} \tag{13}$$

c. For the output component i_{DC}

$$i_{DC} = G_{DC} \left(1 - [1 \quad 1 \quad 1 \quad \cdots \quad 1] \begin{bmatrix} G_{\alpha-1} \\ G_{\alpha-3} \\ G_{\alpha-5} \\ \vdots \\ G_{\alpha-n} \end{bmatrix}^{-1} \begin{bmatrix} G_{\alpha-1} \\ G_{\alpha-3} \\ G_{\alpha-5} \\ \vdots \\ G_{\alpha-n} \end{bmatrix} \right) i_o \tag{14}$$

As it is well known, the harmonics close to the fundamental component (i.e. 3rd, 5th, and 7th harmonics) have a high effect on the output fundamental components than high-order harmonics (far from the fundamental component). Therefore, only the 3rd, 5th, and 7th low harmonics are taken into consideration in the present study, where they will be estimated/rejected from the input fundamental signal of the proposed MESOGI-FLL structure.

Accordingly, the closed-loop transfer functions of the proposed structure regarding the estimation of the output components $i_{\alpha-n}$ and $i_{\beta-n}$ corresponding to the fundamental component, the selected 3rd, 5th, and 7th harmonics, and the DC component can be expressed as follows:

a. For the output components $[i_{\alpha-1}, i_{\alpha-3}, i_{\alpha-5}, i_{\alpha-7}]^T$

$$\begin{bmatrix} i_{\alpha-1} \\ i_{\alpha-3} \\ i_{\alpha-5} \\ i_{\alpha-7} \end{bmatrix} = \begin{bmatrix} G_{BF.\alpha-1} \\ G_{BF.\alpha-3} \\ G_{BF.\alpha-5} \\ G_{BF.\alpha-7} \end{bmatrix} i_o \tag{15}$$

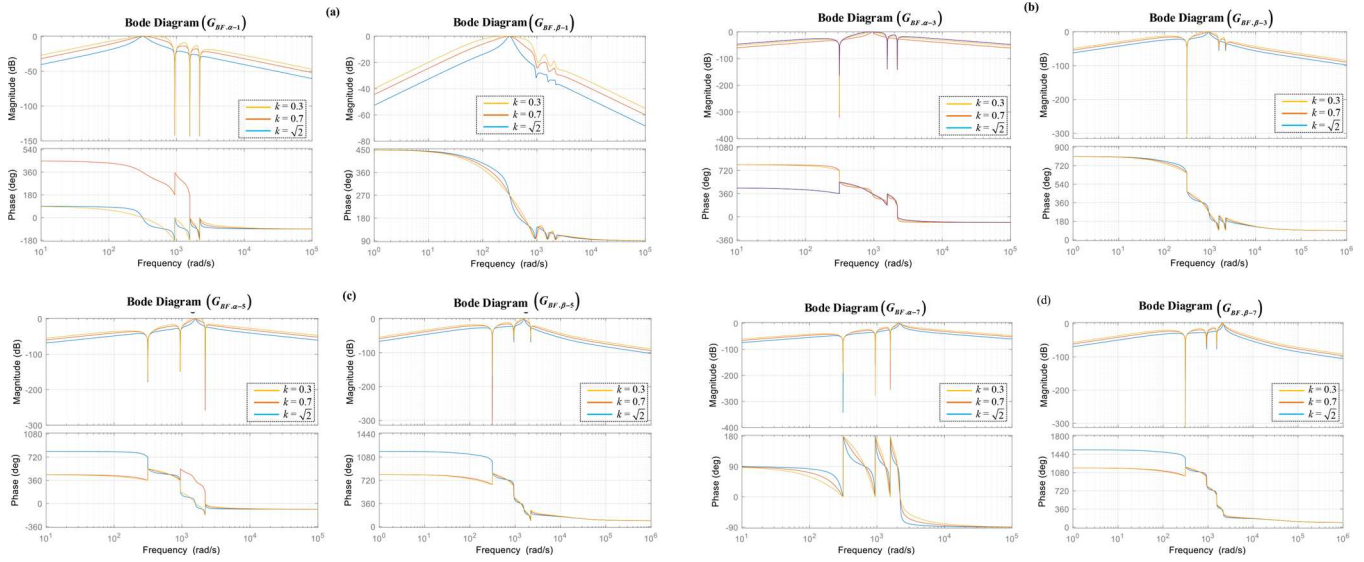


FIGURE 4 Frequency response of the proposed MESOGI-FLL structure regarding the direct and orthogonal output components estimation; (a) fundamental harmonic, (b) 3rd harmonic, (c) 5th harmonic, and (d) 7th harmonic

TABLE 1 Parameters of power calculation methods

Method	Block	Parameters	Symbol	Unit	Value
Proposed Method	ESOGI-QSG, multiple-ESOGI-QSG, MFLL	SOGI-QSG gain	k	—	0.6
		FLL gain	Γ	s^{-1}	50
		LPF cut-off frequency	$\omega_f / 2\pi$	Hz	20
Add-SOGI	SOGI-QSG #0, FLL	SOGI-QSG gain	k_0	—	1
		FLL gain	Γ	s^{-1}	50
	SOGI-QSG #1,2	SOGI-QSG gain	$k_{1,2}$	—	0.707
		LPF	cut-off frequency	$\omega_c / 2\pi$	Hz
SOGI	SOGI-QSG, FLL	SOGI-QSG gain	k	—	0.7
		FLL gain	Γ	s^{-1}	50
		LPF	cut-off frequency	$\omega_c / 2\pi$	Hz
DSOGI	DSOGI-QSG	SOGI-QSG gain	k	—	0.21
n-Order SOGI	n-SOGI-QSG FLL	SOGI-QSG gain	k_v	—	0.7
		SOGI-QSG gain	k_i	—	0.25
		FLL gain	Γ	s^{-1}	50

b. For the output components $[i_{\beta-1}, i_{\beta-3}, i_{\beta-5}, i_{\beta-7}]^T$

$$\begin{bmatrix} i_{\beta-1} \\ i_{\beta-3} \\ i_{\beta-5} \\ i_{\beta-7} \end{bmatrix} = \begin{bmatrix} G_{BF,\beta-1} \\ G_{BF,\beta-3} \\ G_{BF,\beta-5} \\ G_{BF,\beta-7} \end{bmatrix} i_o \quad (16)$$

c. For the output components i_{DC}

$$i_{DC} = G_{BF,DC} \cdot i_o \quad (17)$$

where $G_{BF,\alpha-1,3,5,7}$, $G_{BF,\beta-1,3,5,7}$, and $G_{BF,DC}$ are the transfer functions relating the output orthogonal components and DC component to the actual input current (i_o), and their expressions are given in Appendix B.

The magnitude and phase bode plots of the closed-loop transfer functions $G_{BF,\alpha-1,3,5,7}$ and $G_{BF,\beta-1,3,5,7}$ of the 1st, 3rd, 5th, and 7th harmonics are depicted in Figures 4a–4d, respectively. The frequency response curves; of $G_{BF,\alpha-1,3,5,7}$ and $G_{BF,\beta-1,3,5,7}$; are presented for three different values of the damping factor, $k = 0.3, 0.7$, and $\sqrt{2}$, and $\omega = 2\pi \times 50$ (rad/s). According to these figures, it can be observed that the transfer functions $G_{BF,\alpha-1,3,5,7}$ and $G_{BF,\beta-1,3,5,7}$ exhibit

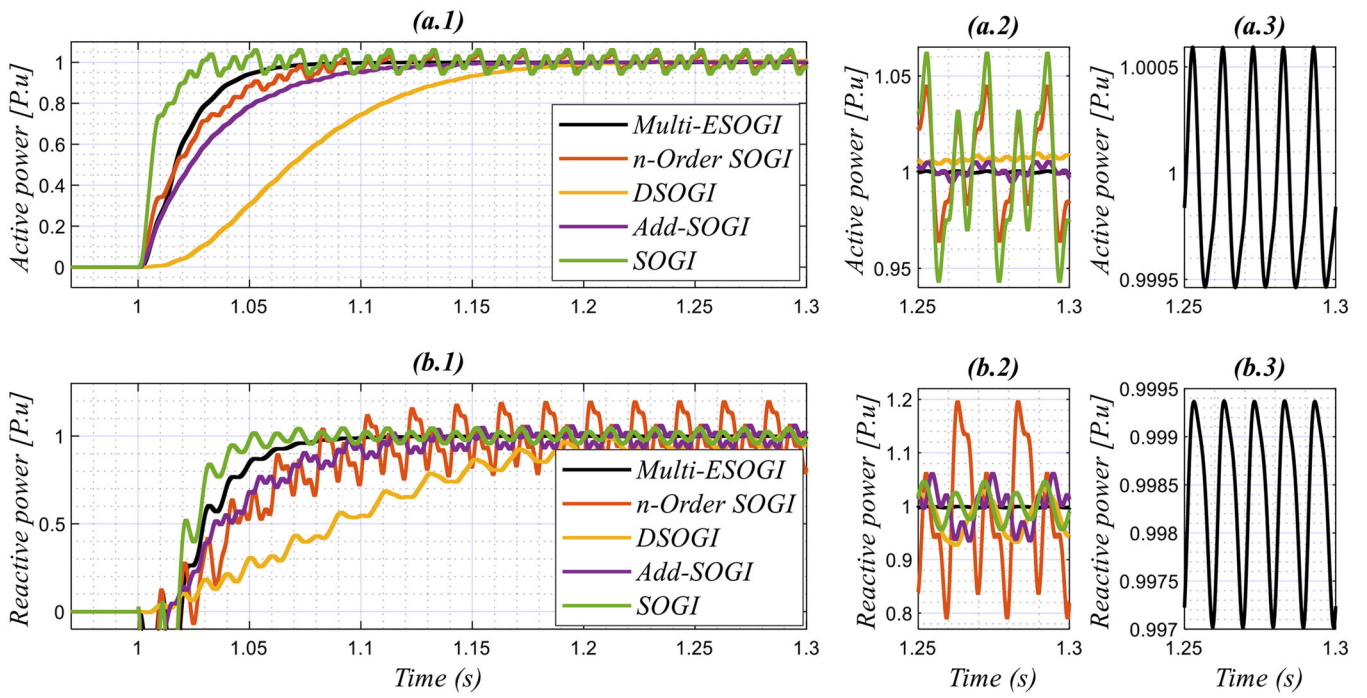


Fig. 6. Obtained results in response to Test 2: (a) active power, and (b) reactive power.

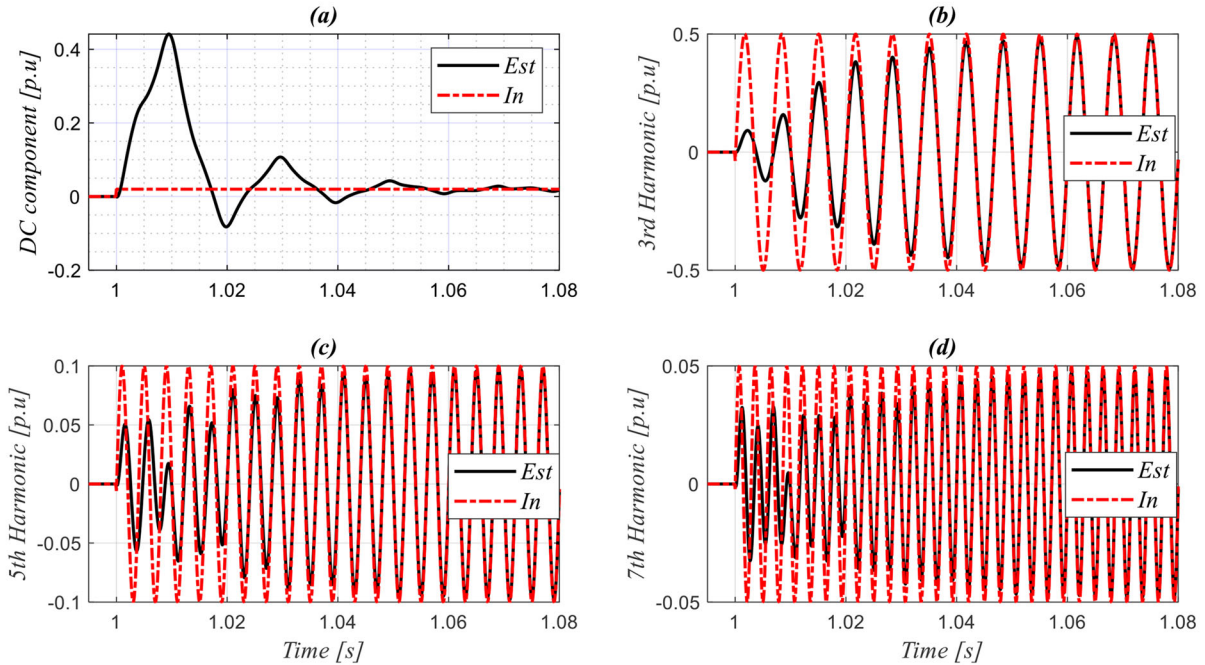


FIGURE 6 Obtained results in response to Test 2: (a) Active power, and (b) reactive power

band-pass adaptive filters where their bandwidth depends on the gain κ .

As can be seen, increasing κ decreases the filter bandwidth, hence, enhancing the filtering capabilities of the sub- and low-harmonics (i.e. 3rd, 5th, and 7th harmonics). But, this effect slows down the speed of the estimates' transient response. Furthermore, from these figures, it can be noticed that the output components $i_{\alpha-1}$, $i_{\alpha-3}$, $i_{\alpha-5}$, and $i_{\alpha-7}$ have the same amplitude and quadrature in the phase with the harmonics set in the input signal (i_o).

As a consequence, the proposed MESOGI-FLL can ensure proper estimation of the direct and quadrature fundamental components, as well as provide good estimation/rejection of the 3rd, 5th, and 7th harmonic and DC components.

3.2 | Comparative study

To assess the performance of the power calculation based on the proposed method in comparison with the other recent methods, a simulation study is carried out in

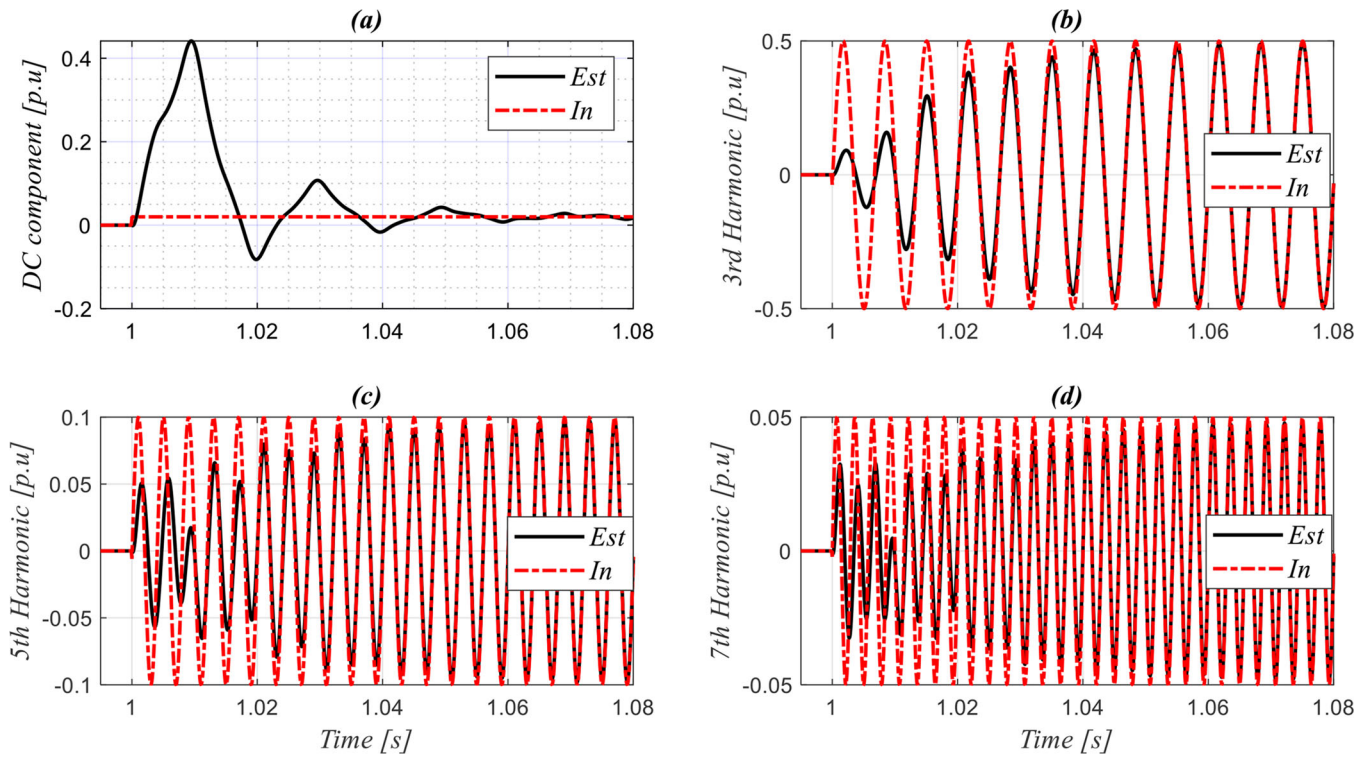


FIGURE 7 MESOGI-FLL estimated and input: (a) DC component, (b) 3rd harmonic, (c) 5th harmonic, and (d) 7th harmonic in response to test 2

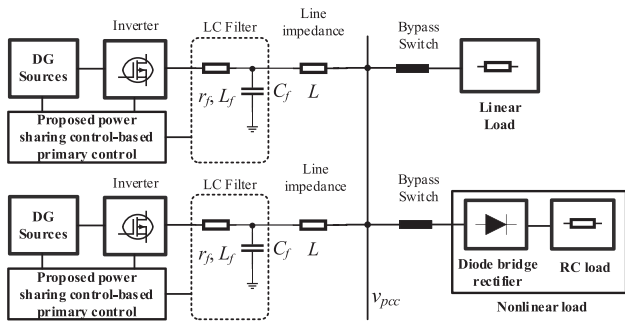


FIGURE 8 Simulated model of the two DG units interfaced micro-grid in MATLAB/Simulink

MATLAB/SIMULINK environment. Here, the performance of the proposed strategy and other methods are evaluated in front of input current and voltage perturbations (without and with DC component and harmonic distortions). The simulations are performed corresponding to the following scenarios:

1. Scenario 1 (pure sinusoidal inputs): In this case, no sub-harmonic and harmonic distortions are induced in the input current and voltage expressed by (18), given below. This test is conducted to highlight the response to an amplitude step change of the inverter current from 0 to 5 A.

$$v_o = V \times \sin(\omega t), i_o = I \times \sin(\omega t - \varphi) \quad (18)$$

TABLE 2 Parameters of the simulation study

Parameters	Symbol	Unit	Value
Nominal voltage (RMS)	E_n	V	220
Nominal frequency	f_n	Hz	50
Switching frequency	f_s	kHz	20
Simulation frequency	f_e	MHz	1
DC voltage	U_{DC}	V	495
Output filter capacitor	C	μF	23
Output filter inductor	L_s, r	mH, Ω	2, 1
Line impedance of DG #1	L_1	mH, Ω	1.5, 0.8
Line impedance of DG #2	L_2	mH, Ω	0.5, 0.8
Virtual inductance	L_v	mH	2.7
Virtual Resistance	R_v	Ω	1
P - ω droop	m	rad/(W. s)	0.0005
Q - V droop	n	V/Var	0.001
Voltage controller P gain	k_{pv}	$\mu\text{F} \cdot \text{rad/s}$	0.1839
Voltage controller I gain	k_{pi}	mH.rad/s	183.87
Current controller P gain	k_{ip}	mH.rad/s	6.2831

2. Scenario 2 (distorted sinusoidal inputs): DC component and harmonic distortions are introduced in the input current and voltage as follows:

3. 2% of the DC component, 10% of the 3rd harmonic, 5% of the 5th harmonic, and 1% of the 7th harmonic from the amplitude of the input voltage (v_o)

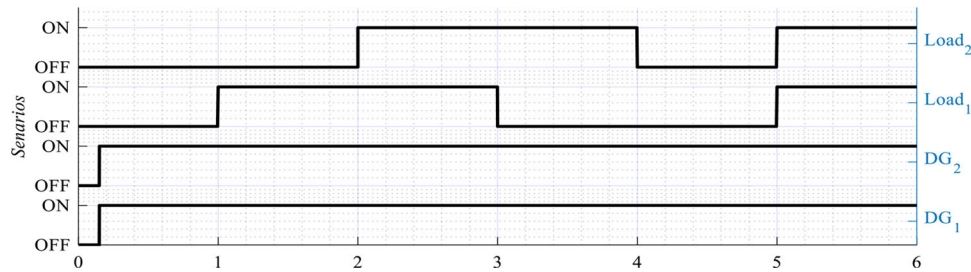


FIGURE 9 Plots of the performed scenarios for test 1

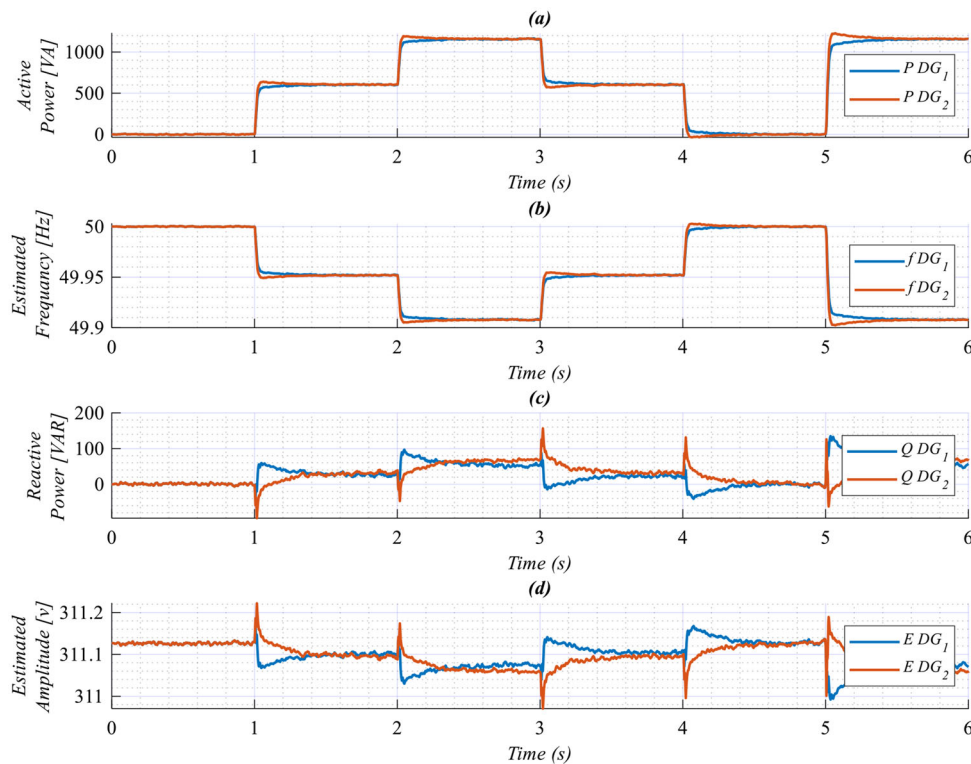


FIGURE 10 Time evolution of (a) active powers, (b) output voltage frequencies, (c) reactive powers, and (d) output voltage amplitudes, of the inverters 1 and 2 in response to linear load change

4. 2 % of the DC component, 50% of the 3rd harmonic, 10% of the 5th harmonic, and 5% of the 7th harmonic form amplitude of the input current (i_o);

Accordingly, the mathematical expressions of v_o and i_o can be given as follows:

$$\begin{aligned}
 v_o &= 0.02V + V \times \sin(\omega t) + 0.1V \times \sin(3\omega t) \\
 &\quad + 0.05V \times \sin(5\omega t) + 0.01V \times \sin(7\omega t) \\
 i_o &= 0.02I + I \times \sin(\omega t - \varphi) + 0.5I \times \sin(3\omega t - \varphi) \\
 &\quad + 0.1I \times \sin(5\omega t - \varphi) + 0.05I \times \sin(7\omega t - \varphi)
 \end{aligned} \tag{19}$$

The parameters for the simulated schemes, in this comparative study, are given in Table 1.

The obtained results of this comparative study in response to scenarios 1 and 2 are illustrated in Figures 5 and 6, respectively. These figures evaluate the P and Q calculation performance obtained by the proposed method compared to those provided by other methods-based schemes, for an input current step change. In addition, Figure 7a–d depicts the transient response of the DC component, 3rd, 5th, and 7th harmonic components estimated by the MESOGI-FLL and the induced ones in the input current given by (19). Based on these simulation results the following remarks can be highlighted.

For scenario 1:

- All the power calculation schemes have the same steady-state responses, in which no ripples in the estimated active and reactive powers.

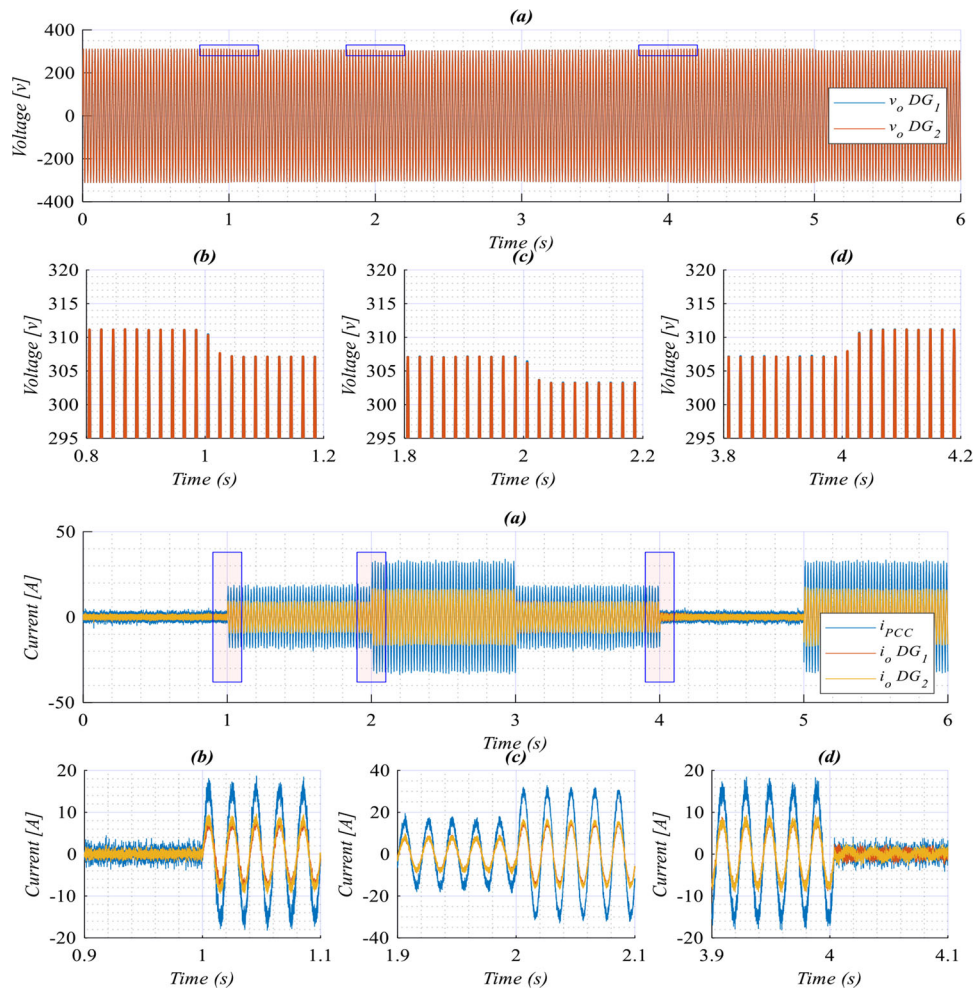


FIGURE 11 Time evolution of the inverters output voltages and currents, and, zooms, in response to linear load change

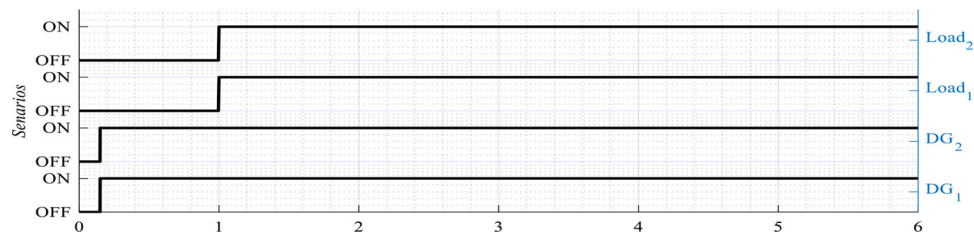


FIGURE 12 Plots of the performed scenarios for test 2

- The SOGI-based P and Q calculation method has the fastest transient response but with significant oscillations, whereas, the method-based DSOGI has the slowest transient response but without any oscillations (very small oscillations in the calculated Q).
- The scheme based on Add-SOGI can achieve the P and Q calculation with a good transient response but with a high settling time, after the one based on DSOGI.
- The proposed scheme is the fastest method for P and Q calculation than the other method, except the one based

on SOGI scheme, and without oscillations in the transient response.

For Scenario 2:

- The performance of the power computation (P and Q) using SOGI- and n-SOGI-based schemes are much affected by the induced DC component and harmonics into the input current and voltage, in which they suffer from higher ripple distortion at steady-state

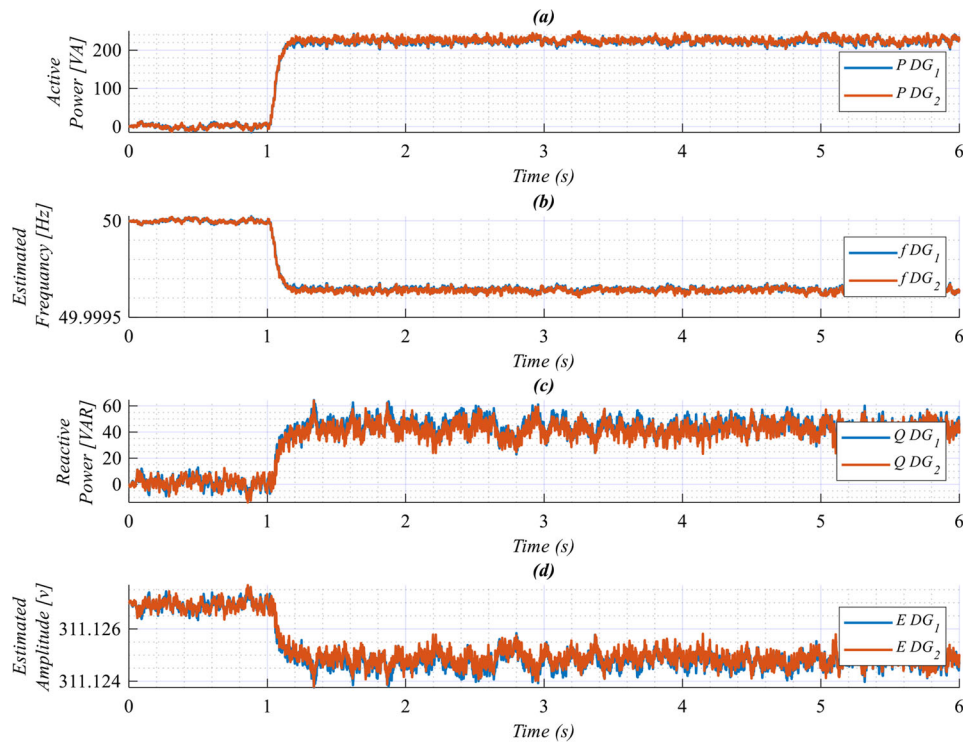


FIGURE 13 The performance of the proposed power control when sharing non-linear load

TABLE 3 VSIs power stages and primary control level parameters

Parameters	Symbol	Unit	Value
Nominal voltage (RMS)	E_n	V	24
Nominal frequency	f_n	Hz	50
Switching frequency	f_s	kHz	10
DC voltage	U_{DC}	V	32
Output filter capacitor	C	μF	26
Output filter inductor	L	mH	2.7
Line impedance of DG #1	L_1	mH	0.5
Line impedance of DG #2	L_2	mH	0.8
Virtual inductance	L_v	mH	4
Virtual Resistance	R_v	Ω	1
P - ω droop	m	rad/(W. s)	0.0003
Q - V droop	n	V/Var	0.003
Voltage controller P gain	k_{pv}	$\mu\text{F}\cdot\text{rad/s}$	0.1307
Voltage controller I gain	k_{pi}	mH.rad/s	32.5476
Current controller P gain	k_{ip}	mH.rad/s	146×10^5
Current controller I gain	k_{ii}	mH.rad/s	1.02×10^5

- The features of the structure based on the DSOGI regarding active power calculation are not influenced by the introduced perturbations, where, less ripple distortions than all the other methods, except the proposed one, are observed (with small oscillations can be noticed in the Q calculation). Despite, these features, this method has a very slow dynamic response.

- The scheme based on Add-SOGI has much lower ripples than the first two methods. However, it has the slowest transient response than the other methods; except the method based on DSOGI.
- The proposed scheme provides improved performances in terms of DC component and harmonics effects rejection in the estimated P and Q . In addition, it has a better settling time than Add-SOGI, n-SOGI, and DSOGI-based schemes.
- It is worth noting that further oscillations are obtained in the estimated reactive power of all the reported methods, except the proposed method that almost has no oscillations.
- The proposed MESOGI-FLL scheme ensures accurate estimation of the DC component and harmonic components of the input current i_o (from Figure 7).

As a consequence, one can be deduced that the proposed scheme can achieve better power calculation performance in terms of the speed of dynamic response, high DC component and harmonics rejection capabilities, and almost no ripples at steady-state, than all the other methods.

4 | SIMULATION RESULTS

In this section, numerical tests are performed in order to assess the effectiveness of the proposed power-sharing control. In these tests, the performance of the proposed control scheme is verified in the case of sharing linear and non-linear loads and during linear load change as well. The testbed considered in the simulations is depicted in Figure 8, and it consists of two

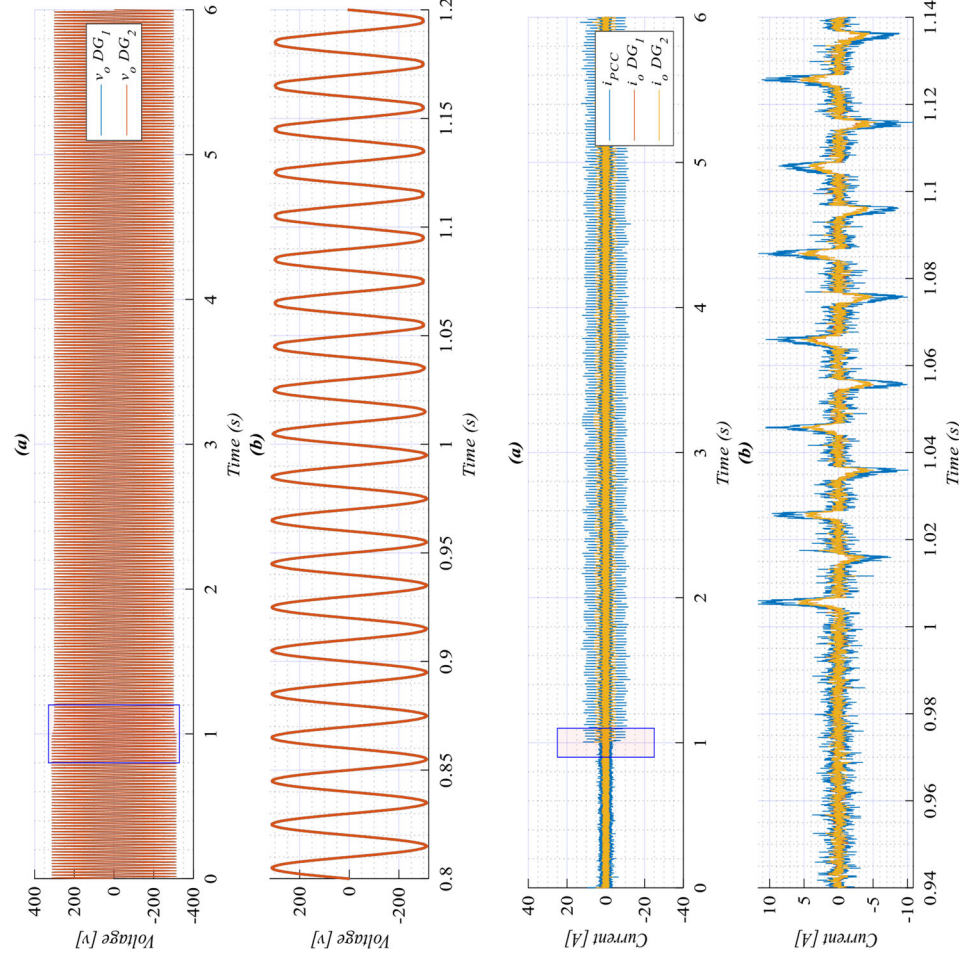


FIGURE 14 The performance of the proposed power control in front of sharing nonlinear load, VSIs output voltages and currents, and zooms

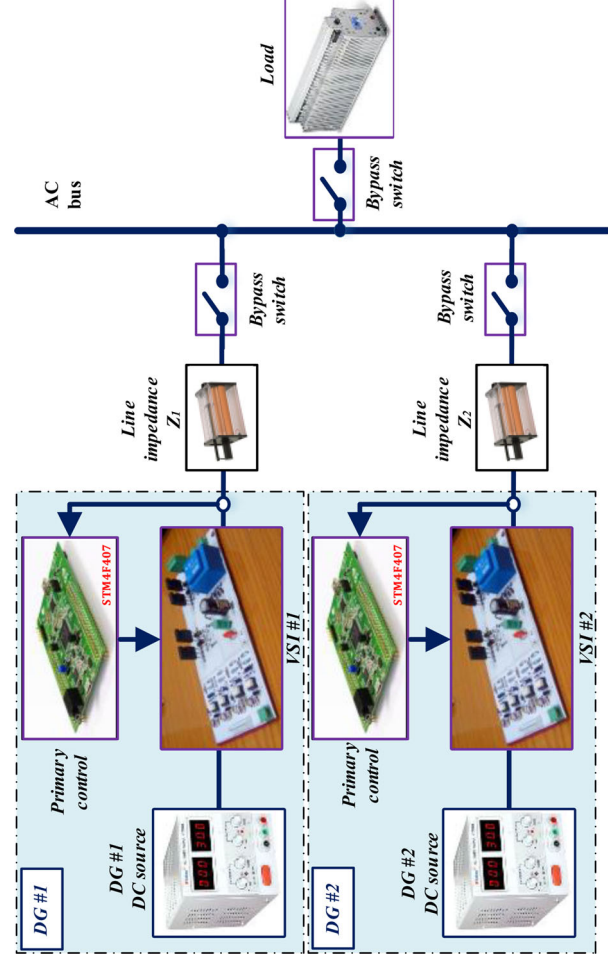


FIGURE 15 The experimental setup of two parallel-connected VSIs

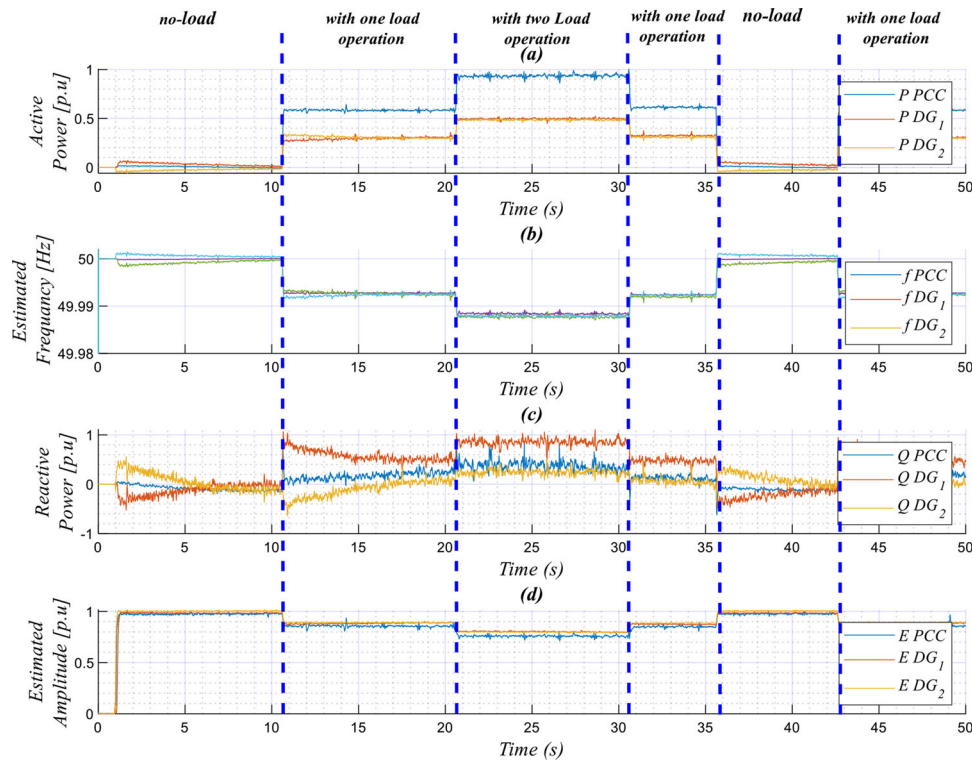


FIGURE 16 Transient responses of the inverters and the load; (a) active powers, (b) frequencies, (c) reactive powers, and (d) amplitudes in response to linear load change

single-phase inverters paralleled-connected to a common AC bus through a line impedance. These inverters supply a critical load and form an islanded microgrid. An RL load (20Ω , 3 mH) is considered as a linear load, while a diode-bridge rectifier feeding an RC load (200Ω , $1000 \mu\text{F}$) represents the nonlinear load. The microgrid system with the proposed control scheme is simulated in SimPowerSystem under the MATLAB/Simulink environment. The proposed power-sharing control stage is given in Figure 1, which includes the improved power calculation method. The main parameters taken for the simulations are given in Table 2. To assess the overall system under a realistic environment, Gaussian noise is added to DC voltage sources and sensors' measurements.

Figure 9 illustrates the performed scenarios for the connection and disconnection of linear loads 1 and 2. The obtained results in response to linear load change are shown in Figures 10 and 11. In these figures, the time responses of the active and reactive power, output voltage amplitude, and frequency, as well as the output voltage and current waveforms of inverters 1 and 2 are presented. First, there is no load connected to the MG, the inverter frequencies and amplitudes are equal and set to their nominal values i. e., $f_{DG1} = f_{DG2} = f_n$ and $E_{DG1} = E_{DG2} = E_n$, while P_{DG1} , P_{DG2} , Q_{DG1} , and Q_{DG2} powers are equal to zero. After, when the first load is connected (at $t = 1 \text{ s}$), the inverters' active and reactive powers increase and the output voltage frequencies (f_{DG1} and f_{DG2}) and amplitudes (E_{DG1} and E_{DG2}) drop, as seen in Figure 10. At $t = 2 \text{ s}$, the second load is connected, the powers seamlessly increase without overshoot and

with reduced settling time (0.02 s). In addition, the amplitudes, E_{DG1} and E_{DG2} , and the frequencies, f_{DG1} , and f_{DG2} , drop even more with the same amount, and with a faster dynamic. Further, it can be noticed that the active power is perfectly shared among the inverters. The same observation can be made for the rest of the scenarios, when the first and the second loads, are disconnected and connected again. It is worth noting that the reactive power in Figure 10 is not constant and varies when the load change. This is due to the increase and decrease of the current passed through the line impedance which leads to a change in the line impedance voltage, and as the reactive power is proportional to the voltage it changes when the load varies.

According to Figure 11, it can be observed that the inverters' output voltages, v_{o-DG1} and v_{o-DG2} , are matched, as well as the currents, i_{o-DG1} and i_{o-DG2} , and have pure sinusoidal forms, also, they change with good transient responses during linear load variations.

The results showing the performance of the proposed controller when the inverters shared nonlinear load are presented in Figures 13 and 14, while Figure 12 presents the performed scenarios. Figures 13 and 14 depict the time evolution of the same variables of test 1. Similar to test 1, the MG system starts with the no-load operation, then, at $t = 1 \text{ s}$ a non-linear load is connected to the MG. As seen in Figure 13, the VSIs' active powers grow and have the same values which mean that they share accurately the load power demand. Also, these powers achieve the rated values respective to load demand, with a fast response time of 0.02 s and without overshoots, and they

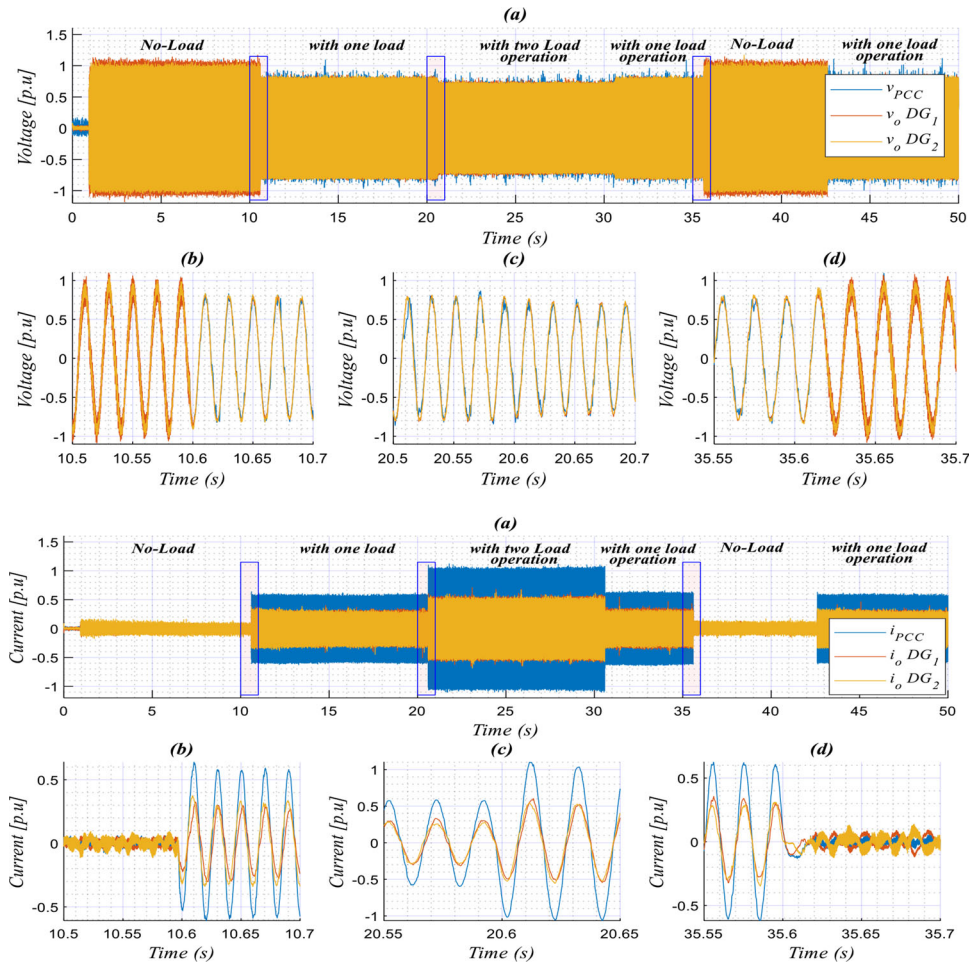


FIGURE 17 Transient responses of the output voltages and currents, and zooms of the VSIs and the load, in the case of linear load change

do not have any ripple distortions or oscillating components in steady-state, even with the distorted currents, as can be seen in Figure 13. Further, the figures demonstrate that f_{DG1} and f_{DG2} droop with the same amounts, showing excellent dynamic response in terms of settling time (0.02 s) and without oscillations, and no ripples are obtained in steady-state as well. Regarding the voltage amplitudes, it can be observed that they increase to compensate for the load reactive power, which is shared between the two VSIs. From the output voltage and current, in this case, shown in Figure 14, one can be noted that the inverters' voltages, v_{o-DG1} and v_{o-DG2} , are matched and have sinusoidal waveforms, while the currents are equal and take the nonlinear load current form to compensate the load reactive power. Moreover, it is clearly appearing that transient responses with good performance are obtained.

5 | EXPERIMENTAL RESULTS

In order to validate the effectiveness of the proposed power-sharing control, an experimental setup of an islanded microgrid is carried out, as shown in Figure 15. The MG is formed by

two single-phase parallel-connected VSIs feed by DC sources, supplying linear or nonlinear loads. A resistive load (20 Ω) is considered for the linear load while the nonlinear load is a full-bridge diode rectifier with an RC load (20 Ω , 470 μF). In this system, the ARM cortex microcontroller (STM32F407VGT6) is chosen as the main control unit with a switching frequency of 10 kHz for implementing the control strategy. Where each VSI's local controller is implemented in a separate microcontroller and without any communication between them. The main parameters taken in the tests are listed in Table 3. The same tests and scenarios as simulation cases are considered but at different times.

The obtained results during transient linear load are given in Figures 16 and 17, which depict the transient response of the active and reactive powers, frequencies, amplitudes, output voltages, and currents of the inverters and the load (at the PCC). According to these figures, one can be seen that at no load the power components and currents are zero, while f_{DG1} , f_{DG2} , E_{DG1} , and E_{DG2} are set to the nominal values. When the loads are added and removed, it can be noticed that active and reactive powers are perfectly shared between the inverters, showing good transient responses in terms of settling time and

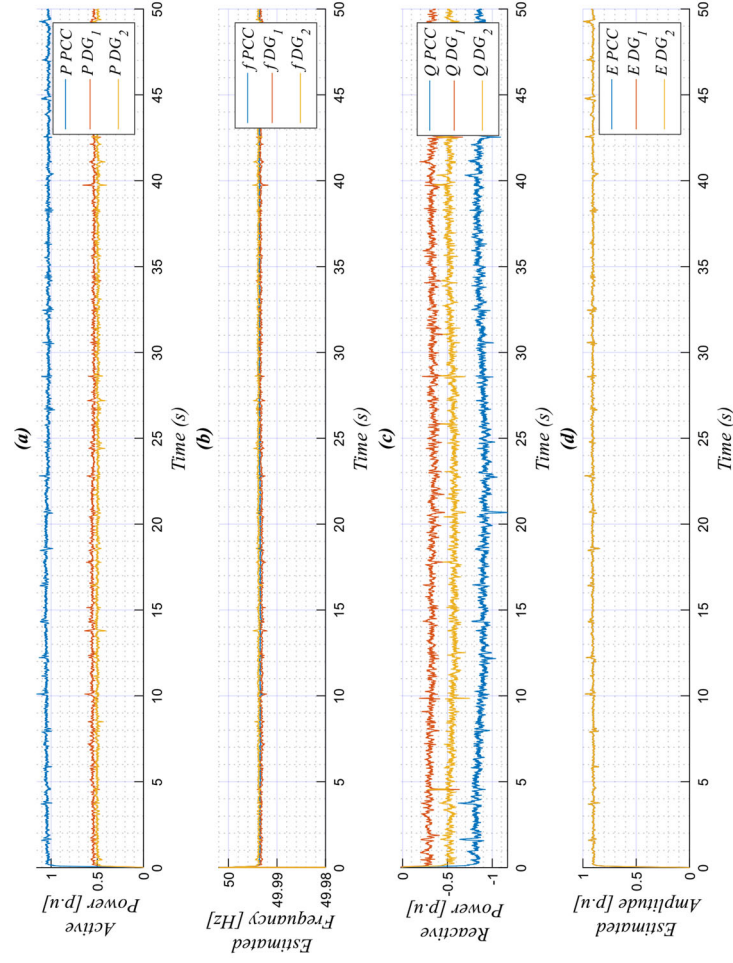


FIGURE 18 Transient responses of the inverters and the load; (a) active powers, (b) frequencies, (c) reactive powers, and (d) amplitudes, for the case of supplying non-linear load

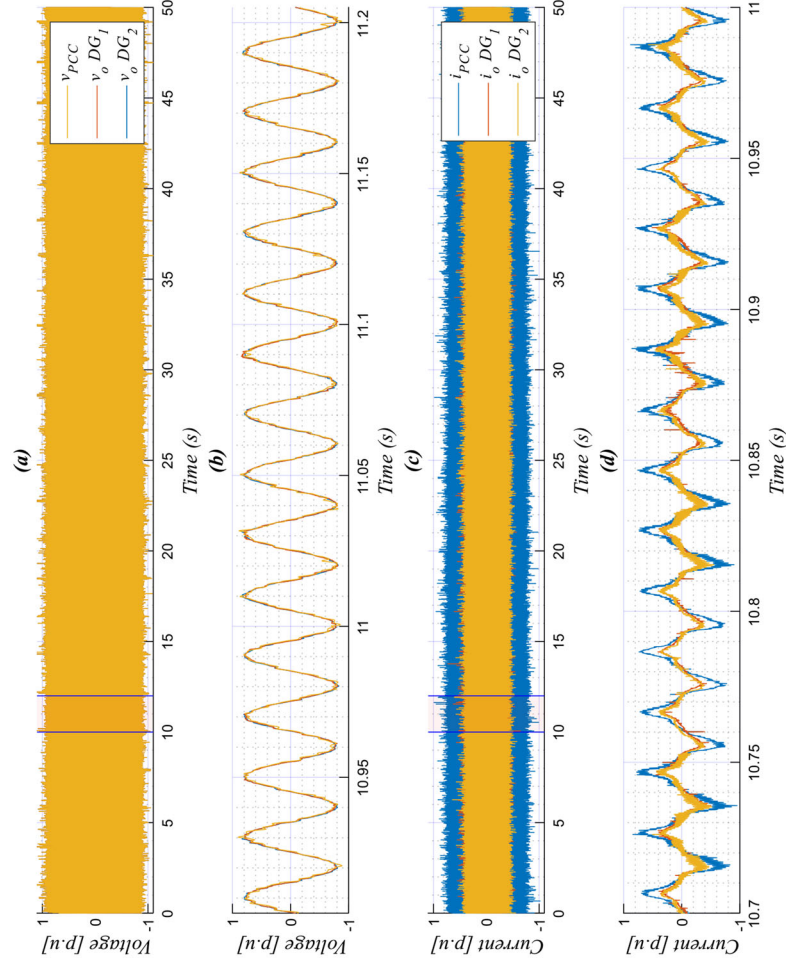


FIGURE 19 Transient responses of the output voltage and currents of the VSI and at the PCC, and zooms, for the case of supplying the non-linear load

no overshoots (see zooms) as well as no ripples at a steady state. Also, the f_{DG1} , f_{DG2} , E_{DG1} , and E_{DG2} droop and grow with the same amounts, respectively, during the load transient to deliver the required load power. Further, they ensure the pure sinusoidal form of the output voltage and current in this case.

Figures 18 and 19 highlight the results obtained in the case of sharing a nonlinear load, and they show the same variables as the first test. In these figures, it can be noted that when the nonlinear load occurs at $t = 0.75$ s, the inverters share accurately the active power delivered to the nonlinear load. In addition, f_{DG1} and f_{DG2} are dropped with equal amounts according to the load demand. The same effect occurs for the reactive powers and amplitudes of the VSIs. Furthermore, the output voltages and currents of the VSIs are matched, in which the currents have the same distorted forms as the load current form. Moreover, the presented figures demonstrate that all obtained variables have good transient responses and steady-state performances.

6 | CONCLUSION

An improved droop-based control strategy, for achieving accurate power-sharing among single-phase parallelized VSIs, considering linear and nonlinear loads, was proposed here. The proposed scheme involves a MESOGI-FLL-based enhanced power calculation method. Computing the averaged powers using multiple ESOGI strategy-based power calculation was performed and verified. It is worth mentioning here that the use of MESOGI-FLL leads to an accurate P/Q calculation with fast transient response and low computational cost compared to the reported recent methods. The mathematical model of MSOGI and its analysis has been derived in this work. In addition, the proposed power calculation method has been compared to some relevant reported power calculation methods. A performance comparison between the proposed method and these power calculation methods under normal and distorted operating conditions was then conducted. The simulation and experimental findings confirm that the proposed method offers proper power calculation with high rejection capability for DC component and current distortions and a good trade-off relationship between harmonic rejection and transient response speed.

AUTHOR CONTRIBUTIONS

A.B.: Conceptualization; Formal analysis; Investigation; Methodology; Software; Validation; Visualization; Writing - original draft; Writing - review and editing

ACKNOWLEDGEMENTS

The work of H. Ahmed is funded through the Sêr Cymru II 80761-BU-103 project by Welsh European Funding Office (WEFO) under the European Regional Development Fund (ERDF).

CONFLICT OF INTEREST

The authors declare no conflict of interest.

DATA AVAILABILITY STATEMENT

The data that support the findings of this study are available from the corresponding author upon reasonable request.

ORCID

Abdelhamid Kherbachi  <https://orcid.org/0000-0002-6166-7744>

Hafiz Ahmed  <https://orcid.org/0000-0001-8952-4190>

REFERENCES

- Guerrero, J.M., Vasquez, J.C., Matas, J., de Vicuna, L.G., Castilla, M.: Hierarchical control of droop-controlled ac and dc microgrids—a general approach toward standardization. *IEEE Trans. Ind. Electron.* 58(1), 158–172 (2011)
- Vasquez, J.C., Guerrero, J.M., Savaghebi, M., Eloy-Garcia, J., Teodorescu, R.: Modeling, analysis, and design of stationary-reference-frame droop-controlled parallel three-phase voltage source inverters. *IEEE Trans. Ind. Electron.* 60(4), 1271–1280 (2013)
- Zhong, Q.C.: Robust droop controller for accurate proportional load sharing among inverters operated in parallel. *IEEE Trans. Ind. Electron.* 60(4), 1281–1290 (2013) <https://doi.org/10.1109/TIE.2011.2146221>
- Dehkordi, N.M., Sadati, N., Hamzeh, M.: Robust tuning of transient droop gains based on Kharitonov's stability theorem in droop-controlled microgrids. *IET Gener. Transm. Distrib.* 12(14), 3495–3501 (2018)
- Peng, J.C.-H., Raman, G., Soon, J.L., Hatzigiargyriou, N.D.: Droop-Controlled Inverters as Educational Control Design Project. *IEEE Trans. Power Systems* 37(2), 1623–1633 (2022)
- Vasquez, J.C., Guerrero, J.M., Luna, A., Rodriguez, P., Teodorescu, R.: Adaptive droop control applied to voltage-source inverters operating in grid-connected and islanded modes. *IEEE Trans. Ind. Electron.* 56(10), 4088–4096 (2009)
- Minetti, M., Rosini, A., Denegri, G.B., Bonfiglio, A., Procopio, R.: An advanced droop control strategy for reactive power assessment in islanded microgrids. *IEEE Trans. Power Systems* 37(4), 3014–3025 (2022)
- El-Mariachet, J., Guan, Y., Matas, J., Martín, H., Li, M., Guerrero, J.M.: HIL-assessed fast and accurate single-phase power calculation algorithm for voltage source inverters supplying to high total demand distortion nonlinear loads. *Electronics* 9(10), 1643 (2020)
- Guerrero, J.M., de Vicuna, L.G., Matas, J., Castilla, M., Miret, J.: A wireless controller to enhance dynamic performance of parallel inverters in distributed generation systems. *IEEE Trans. Power Electron.* 19(5), 1205–1213 (2004)
- Yu, W., Xu, D., Ma, K.: A novel accurate active and reactive power calculation method for paralleled ups system. In: 2009 Twenty-Fourth Annual IEEE Applied Power Electronics Conference and Exposition (APEC), pp. 1269–1275. Washington, DC, USA (2009)
- Guerrero, J.M., Matas, J., Garcia de Vicuna, L., Castilla, M., Miret, J.: Decentralized control for parallel operation of distributed generation inverters using resistive output impedance. *IEEE Trans. Ind. Electron.* 54(2), 994–1004 (2007)
- Alcala, J.M., Castilla, M., de Vicuña, L.G., Miret, J., Vasquez, J.C.: Virtual impedance loop for droop-controlled single-phase parallel inverters using a second-order general-integrator scheme. *IEEE Trans. Power Electron.* 25(12), 2993–3002 (2010)
- Ren, Z., et al.: Power calculation method used in wireless parallel inverters under nonlinear load conditions. In: 2010 Twenty-Fifth Annual IEEE Applied Power Electronics Conference and Exposition (APEC), pp. 1674–1677. Palm Springs, CA, USA (2010)
- Andrade, E.T., Ribeiro, P.E.M.J., Pinto, J.O.P., Chen, C., Lai, J., Kees, N.: Novel power calculation method for droop-control microgrid systems. In: 2012 Twenty-Seventh Annual IEEE Applied Power Electronics Conference and Exposition (APEC), pp. 2254–2258. Orlando, FL, USA (2012)
- Kherbachi, A., Bendib, A., Kara, K., Chouder, A.: ARM-based implementation of SOGI-FLL method for power calculation in single-phase power

- system. In: 2017 5th International Conference on Electrical Engineering - Bumerdes (ICEE-B), pp. 1–6. Bumerdes, Algeria (2017)
16. Lu, J., Wen, Y., Zhang, Y., Wen, W.: A novel power calculation method based on second-order general integrator. In: 2016 IEEE 8th International Power Electronics and Motion Control Conference (IPEMC-ECCE Asia), pp. 1975–1979. Hefei, China (2016)
 17. Bendib, A., Chouder, A., Kara, K., Kherbachi, A., Barkat, S., Walid, W.: New modeling approach of secondary control layer for autonomous single-phase microgrids. *J. Franklin Inst.* 356(13), 6842–6874 (2019)
 18. Tolani, S., Sensarma, P.: An improved droop controller for parallel operation of single-phase inverters using R-C output impedance. In: 2012 IEEE International Conference on Power Electronics, Drives and Energy Systems (PEDES), pp. 1–6. Bengaluru, India (2012)
 19. Azevedo, G.M.S., Cavalcanti, M.C., Bradaschia, F., Neves, F.A.S., Rocabert, J., Rodriguez, P.: Enhanced power calculator for droop control in single-phase systems. In: 2011 IEEE Energy Conversion Congress and Exposition, pp. 391–396. Phoenix, AZ, USA (2011)
 20. Yang, Y., Blaabjerg, F., Wang, H.: Low-voltage ride-through of single-phase transformerless photovoltaic inverters. *IEEE Trans. Ind. Appl.* 50(3), 1942–1952 (2014)
 21. Yang, Y., Blaabjerg, F.: A new power calculation method for single-phase grid-connected systems. In: 2013 IEEE International Symposium on Industrial Electronics. pp. 1–6. Taipei, Taiwan (2013)
 22. Mota, D.D.S., Tedeschi, E.: On adaptive moving average algorithms for the application of the conservative power theory in systems with variable frequency. *Energies*. 14(4), 1201 (2021)
 23. El Mariachet, J., Matas, J., de la Hoz, J., Al-Turki, Y., Abdalgader, H.: A power calculation algorithm for single-phase droop-operated-inverters considering linear and nonlinear loads HIL-assessed. *Electronics* 8(11), 1366 (2019)
 24. Kherbachi, A., Chouder, A., Bendib, A., Kara, K., Barkat, S.: Enhanced structure of second-order generalized integrator frequency-locked loop suitable for DC-offset rejection in single-phase systems. *Electr. Power Syst. Res.* 170, 348–357 (2019)
 25. Li, M., Matas, J., Mariachet, J.E., Branco, C.G.C., Guerrero, J.M.: A fast power calculation algorithm for three-phase droop-controlled-inverters using combined SOGI filters and considering nonlinear loads. *Energies*. 15(19), 7360 (2022)
 26. Bendib, A., Kherbachi, A., Chouder, A., Ahmed, H., Kara, K.: Advanced control scheme and dynamic phasor modeling of grid-tied droop-controlled inverters. *IET Renewable Power Gener.* 1–19 (2022). <https://doi.org/10.1049/rpg2.12610>
 27. El Mariachet, J., Matas, J., de la Hoz, J., Al-Turki, Y., Abdalgader, H.: Power calculation algorithm for single-phase droop-operated inverters considering nonlinear loads and using n-order SOGI filtering. In: 2018 International Conference on Renewable Energies and Power Quality (ICREPQ), pp. 710–715. Salamanca, Spain (2018)
 28. Akhavan, A., Golestan, S., Vasquez, J.C., Guerrero, J.M.: Passivity enhancement of voltage-controlled inverters in grid-connected microgrids considering negative aspects of control delay and grid impedance variations. *IEEE J. Emerging Sel. Top. Power Electron.* 9(6), 6637–6649 (2021)

How to cite this article: Kherbachi, A., Chouder, A., Bendib, A., Ahmed, H.: Improved power computation method for droop-controlled single-phase VSIs in standalone microgrid considering non-linear loads. *IET Gener. Transm. Distrib.* 17, 1442–1460 (2023). <https://doi.org/10.1049/gtd2.12749>

APPENDIX A

In this appendix, we give the demonstration that describes how the gain k of the ESOGI corresponding to the harmonics'

estimation, is selected. As mentioned above, the gain k of the ESOGI blocks of the harmonic estimates is divided by the order of the harmonic component, n , to keep the same settling time of transient responses of all the ESOGI blocks.

Indeed, it is well known that the settling time, t_{s-b1} , of a second-order transfer function, can be defined as a function of its resonance pulsation ω_r and damping factor k as follows (for ESOGI corresponding to the fundamental component estimation):

$$t_{s-b1} = \frac{4}{\frac{k}{2}\omega_{r-b1}} \quad (A1)$$

Accordingly, the expression of the settling time, t_{s-bn} , corresponding to the n -order harmonics can be obtained as follows:

$$t_{s-bn} = \frac{4}{\frac{k_{bn}}{2}\omega_{r-bn}} = \frac{4}{\frac{k_{bn}}{2}(n \times \omega_{r-b1})} \quad (A2)$$

where ω_{n-bn} is the resonance frequency of the ESOGI corresponding to the n -order harmonic estimation, which is equal to $n \times \omega_{n-b1}$.

In order to maintain the same settling time as that of the fundamental component estimation dynamic, i.e., $t_{s-bn} = t_{s-b1}$, the expression of the gain k_{bn} of each unit should be defined as follows:

$$k_{bn} = \frac{k}{n} \quad (A3)$$

APPENDIX B

In this appendix, the closed-loop transfer functions; $G_{BF.\alpha-1,3,5,7}$, $G_{BF.\beta-1,3,5,7}$, and $G_{BF.DC}$; that relate the output current components of the MESOGI-FLL; i.e., direct, quadrature, fundamental, and DC components; to the actual input current are provided. These transfer functions can be defined as follows:

$$\begin{aligned} \bullet \quad G_{BF.\alpha-1} &= \frac{k\omega s^7 + 83k\omega^3 s^5 + 1891k\omega^5 s^3 + 11025k\omega^7 s}{Den(1)} \\ \bullet \quad G_{BF.\alpha-3} &= \frac{k\omega s^7 + 75k\omega^3 s^5 + 1299k\omega^5 s^3 + 1225k\omega^7 s}{Den(1)} \\ \bullet \quad G_{BF.\alpha-5} &= \frac{k\omega s^7 + 59k\omega^3 s^5 + 499k\omega^5 s^3 + 441k\omega^7 s}{Den(1)} \\ \bullet \quad G_{BF.\alpha-7} &= \frac{k\omega s^7 + 35k\omega^3 s^5 + 259k\omega^5 s^3 + 225k\omega^7 s}{Den(1)} \\ \bullet \quad G_{BF.\beta-1} &= \frac{k\omega^2 s^6 + 83k\omega^4 s^4 + 1891k\omega^6 s^2 + 11025k\omega^8}{Den(1)} \\ \bullet \quad G_{BF.\beta-3} &= \frac{3k\omega^2 s^6 + 225k\omega^4 s^4 + 3897k\omega^6 s^2 + 3675k\omega^8}{Den(1)} \\ \bullet \quad G_{BF.\beta-5} &= \frac{5k\omega^2 s^6 + 295k\omega^4 s^4 + 2495k\omega^6 s^2 + 2205k\omega^8}{Den(1)} \\ \bullet \quad G_{BF.\beta-7} &= \frac{7k\omega^2 s^6 + 245k\omega^4 s^4 + 1813k\omega^6 s^2 + 1575k\omega^8}{Den(1)} \\ \bullet \quad G_{BF.DC} &= \frac{\omega_f s^8 + 84\omega^2 \omega_f s^6 + 1974\omega^4 \omega_f s^4 + 12916\omega^6 \omega_f s^2 + 11025\omega^8 \omega_f}{Den(2)} \end{aligned} \quad (A4)$$

where:

$$Den(1) = s^8 + 4k\omega s^7 + 84\omega^2 s^6 + 252k\omega^3 s^5 + 1974k\omega^4 s^4 + \dots \\ 3948k\omega^5 s^3 + 12916\omega^6 s^2 + 12916k\omega^7 s + 11025\omega^8 \quad (A5)$$

$$Den(2) = s^9 + (\omega_f + 4k\omega) s^8 + (84\omega^2 + 4k\omega\omega_f) s^7$$

$$+ (252k\omega^3 + 84\omega^2\omega_f) s^6 \dots$$

$$+ (1974\omega^4 + 252k\omega^3\omega_f) s^5$$

$$+ (3948k\omega^5 + 1974\omega^4\omega_f) s^4 + \dots$$

$$(12916\omega^6 + 3948k\omega^5\omega_f) s^3$$

$$+ 12916(k\omega^7 + \omega^6\omega_f) s^2 + \dots$$

$$(11025\omega^8 + 12916k\omega^6\omega_f) s + 11025\omega^8\omega_f$$

(A6)